



OPEN ACCESS

EDITED BY

Balkrishna Chaube,
Yale University, United States

REVIEWED BY

Parul Singh,
Immunology Center, National Heart,
Lung, and Blood Institute (NIH),
United States
Suyasha Roy,
National Institutes of Health (NIH),
United States

*CORRESPONDENCE

Aiguo Shen
✉ aiguoshen_nt@126.com

[†]These authors have contributed
equally to this work

SPECIALTY SECTION

This article was submitted to
Cancer Metabolism,
a section of the journal
Frontiers in Oncology

RECEIVED 26 October 2022

ACCEPTED 05 December 2022

PUBLISHED 21 December 2022

CITATION

Liu Y, Lin W, Yang Y, Shao J, Zhao H,
Wang G and Shen A (2022) Role of
cuproptosis-related gene in lung
adenocarcinoma.
Front. Oncol. 12:1080985.
doi: 10.3389/fonc.2022.1080985

COPYRIGHT

© 2022 Liu, Lin, Yang, Shao, Zhao,
Wang and Shen. This is an open-access
article distributed under the terms of
the [Creative Commons Attribution
License \(CC BY\)](https://creativecommons.org/licenses/by/4.0/). The use, distribution
or reproduction in other forums is
permitted, provided the original
author(s) and the copyright owner(s)
are credited and that the original
publication in this journal is cited, in
accordance with accepted academic
practice. No use, distribution or
reproduction is permitted which does
not comply with these terms.

Role of cuproptosis-related gene in lung adenocarcinoma

Yuan Liu^{1†}, Wei Lin^{2†}, Ying Yang^{1†}, JingJing Shao¹,
Hongyu Zhao³, Gaoren Wang¹ and Aiguo Shen^{1*}

¹Cancer Research Center Nantong, Affiliated Tumor Hospital of Nantong University, Nantong, China,

²Department of Pediatrics, the First Affiliated Hospital, Fujian Medical University, Fuzhou, China,

³Department of Radiotherapy, Affiliated Hospital of Nantong University, Nantong, Jiangsu, China

Backgrounds: Lung adenocarcinoma (LUAD) is the most common subtype of lung cancer, which is the leading cause of cancer death. Dysregulation of cell proliferation and death plays a crucial role in the development of LUAD. As of recently, the role of a new form of cell death, cuproptosis, and it has attracted more and more attention. As of yet, it is not clear whether cuproptosis is involved in the progression of LUAD.

Methods: An integrated set of bioinformatics tools was utilized to analyze the expression and prognostic significance of cuproptosis-related genes. Meanwhile, a robust risk signature was developed using machine learning based on prognostic cuproptosis-related genes and explored the value of prognostic cuproptosis-related signature for clinical applications, functional enrichment and immune landscape. Lastly, the dysregulation of the cuproptosis-related genes in LUAD was validated by *in vitro* experiment.

Results: In this study, first, cuproptosis-related genes were found to be differentially expressed in LUAD patients of public databases, and nine of them had prognostic value. Next, a cuproptosis-related model with five features (DLTA, MTF1, GLS, PDHB and PDHA1) was constructed to separate the patients into high- and low-risk groups based on median risk score. Internal validation set and external validation set were used for model validation and evaluation. What's more, Enrichment analysis of differential genes and the WGCNA identified that cuproptosis-related signatures affected tumor prognosis by influencing tumor immunity. Small molecule compounds were predicted based on differential expressed genes to improve poor prognosis in the high-risk group and a nomogram was constructed to further advance clinical applications. In closing, our data showed that FDX1 affected the prognosis of lung cancer by altering the expression of cuproptosis-related signature.

Conclusion: A new cuproptosis-related signature for survival prediction was constructed and validated by machine learning algorithm and *in vitro*

experiments to reflect tumor immune infiltration in LUAD patients. The purpose of this article was to provide a potential diagnostic and therapeutic strategy for LUAD.

KEYWORDS

cuproptosis, lung adenocarcinoma, immune infiltration, prognostic signature, immune microenvironment

1 Introduction

As the highest mortality rate and incidence of the second highest rate in the world, lung cancer has a 5-year survival rate of only 26% (1). Lung adenocarcinoma (LUAD), one of the most prevalent subtype in non-small cell lung cancer (NSCLC), accounts for approximately 40% of lung cancers (2). Despite rapid advances in treatment options including chemotherapy, radiotherapy and surgery, the prognosis for LUAD-patients remains unsatisfactory. Over the past few years, immune checkpoint inhibitor (ICI) therapy has emerged as a revolutionary form of cancer treatment that works by targeting immune checkpoints (3). And yet, only a fraction of patients had achieved expected benefit from ICI therapy. To optimize the prognosis and benefit of LUAD pharmacotherapy, reliable biomarkers are required in the era of individualized therapy. Classical clinical models predict the prognosis of LUAD predicted by tumor extension, performance status, TNM staging and pathological staging indicators, but the heterogeneity of LUAD had prevented these models from achieving satisfactory results (4). Therefore, new models need to be constructed for the treatment and prognosis of LUAD.

Proliferation and death of cells are dysregulated in LUAD. Massive cell death is often a precursor to disease progression, followed by an imbalance between cell proliferation and death resulting in tumor growth (5). According to a recent research in Science, an accumulation of intracellular copper ions triggered the aggregation of Fe-S cluster proteins and destabilization of mitochondrial lipidated proteins, leading to a unique type of cell death called cuproptosis (6). On the one hand, elevated copper levels in LUAD patients could promote tumor angiogenesis, progression and metastasis (7). On the other hand, mitochondria could influence cancer drug resistance, leading to poorer chemotherapy outcomes in LUAD patients (8).

The current prevailing doctrine is that treatment failure in lung adenocarcinoma is the result of resistance to apoptosis (9). Although several studies have validated the ability of cuproptosis-related genes to affect the prognosis of lung adenocarcinoma patients by bioinformatics techniques, the

mechanism has not been fully elucidated (10–13). Therefore, it might be important to explore the role of cuproptosis-related genes in LUAD.

In the current work, five prognostic cuproptosis-related genes (PCRGs) were identified in LUAD. A signature based on PCRGs was constructed and validated for clinical applications and related mechanisms by machine learning algorithm and *in vitro* experiments. Our findings were expected to provide a valuable diagnostic and therapeutic strategies for LUAD patients.

2 Materials and methods

2.1 Data collection and sample pre-processing for LUAD patients

RNA sequencing, survival data, and clinical phenotypes were collected from The Cancer Genome Atlas (TCGA) database in University of California Santa Cruz (UCSC) Xena platform (<http://www.genome.ucsc.edu/>). After data cleaning and normalization, a total of 442 tumor tissues and 49 paracancerous tissues were enrolled. Meanwhile, the normal tissues from Genotype-Tissue Expression (GTEx) (<https://www.gtexportal.org>) were obtained. In addition, a total of 332 patients with survival time and mRNA expression matrix were download from GSE31210 (246) and GSE30219 (86) in Gene Expression Omnibus database (GEO, <https://www.ncbi.nlm.nih.gov/geo/>), and 301 patients with survival time clinical data were collected from Affiliated Tumor Hospital of Nantong University.

2.2 Consensus clustering

Unsupervised clustering was performed using The “ConsensusClusterPlus” R package. A consensus clustering approach (Euclidean distance) was run by K-means clustering algorithm for 1000 times with a resampling rate of 80%. An empirical cumulative distribution function plot was used to Identified the optimal number of clusters.

2.3 Construction of cuproptosis-related signature

First, univariate Cox regression identified PCRGs in the TCGA-LUAD cohort. Subsequently, least absolute shrinkage and selection operator (LASSO) algorithm were performed on the PCRGs in TCGA-LUAD cohort. Finally, the cuproptosis-related signature was constructed by the stepwise Cox regression algorithm. Risk score = $\sum_{i=1}^n \text{Coef}(\text{Gene}) \times \text{Expr}(\text{Gene})$. Coef is the coefficient, Expr is the Fragments Per Kilobase of exon Model per million mapped fragments (FPKM) of each gene. LUAD patients with risk-score above the median were categorized as the high-risk subgroup, and the rest were included in the low-risk subgroup. For model, the time-dependent receiver operating characteristic (ROC) was calculated across validation datasets. Survival analysis was used “survival”, “survminer” and “timeROC” packages, and the nomogram was used “rms” package. The ROC curve, the Harrell’s concordance index (C-index), calibration curve and detrended correspondence analysis (DCA) were performed to evaluate the performance of the nomogram.

2.4 Identification of differentially expressed genes

The threshold value for screening differential genes was set to $|\log_2\text{FC}| > 1$ and adjusted $P < 0.05$. The threshold for stepwise-Cox analysis was set to $P < 0.1$ to screen the final pcrg. Paired samples of cancer tissue and paraneoplastic tissue from TCGA were used to test spatial differences in gene expression in the same individual. Human Protein Atlas database was used for the purpose of examining the expression of cuproptosis-related signature at the protein level (<https://www.proteinatlas.org/>).

2.5 Weighted correlation network analysis

The co-expression network of TCGA-LUAD was generated using the weighted gene weighted gene co-expression network analysis (WGCNA) package. A suitable soft threshold β is calculated based on the criteria for scale-free networks. In the following step, the weighted adjacency matrix was converted into a topological overlap matrix (TOM), and the corresponding dissimilarity (1-TOM) was calculated. Module identification was conducted using the dynamic tree cutting approach. The modules most relevant to the clinical phenotype of the risk score were selected for subsequent analysis.

2.6 Gene network and enrichment analysis of PCRGs

The gene network analysis was performed using GENEMANIA to analyze potential interactions between these genes (<http://genemania.org/>). In order to explore the potential mechanisms and pathways between the riskscore subgroups and two clusters, the Gene ontology (GO), Kyotoencyclopedia of genes and genomes (KEGG) functional enrichment analysis, and gene set enrichment analysis (GSEA), gene set variation analysis (GSVA) were conducted among DEGs between the riskscore subgroups and clusters using the R packages “clusterProfiler”, “enrichplot”, “limma”, “ggplot2”, and “org.Hs.eg.db”.

2.7 Analysis of immune infiltration

“CIBERSORT” algorithm was used to assess the infiltration of 22 immune cells. Four other algorithms such as xcell, MCP-counter, GSVA, and ESTIMATE, were used to verify the robustness of CIBERSORT algorithm. The immune checkpoints were based on published research (14). The expression of HLA gene were used to assess the capabilities of antigen-presentation response.

2.8 Therapeutic response and drug prediction

In order to estimate the likelihood of drug interactions, the DEGs was identified from the high- and low-risk subgroups. L1000FWD (<https://maayanlab.cloud/L1000FWD/>) database was used to detect the signaling pathways affected by small molecule drugs. PubChem database was used for visualizing the structure of drugs (<https://pubchem.ncbi.nlm.nih.gov/>).

2.9 Clinical specimens

Written informed consent was obtained from all patients involved in this study. The ethics committee of the Affiliated Tumor Hospital of Nantong University approved this study.

2.9.1 Quantitative real time PCR

The LUAD and paired para-cancerous samples were collected from 4 patients who underwent lobectomy between August 2022 and October 2022 at Affiliated Tumor Hospital of Nantong University. RNA were extracted and reverse transcription as previously described (15). After reverse transcription, quantitative real time PCR (qRT-PCR) was performed. The primer sequences were shown in Table 1.

TABLE 1 Primers used qRT-PCR detection.

| GENE | PRIMER | SEQUENCE (5'-3') |
|-------|---------|-------------------------------|
| PDHA | Forward | tac agg atg atg cag act gta c |
| | Reverse | caa gtg aca gaa acc acg aat a |
| PDHB | Forward | gac act ccc ata tca gag atg g |
| | Reverse | ctt ggc agc tga gtt tat aac c |
| GLS | Forward | cac tca aat cag gat tgc g |
| | Reverse | cca gac tgc ttt tta gca ctt t |
| MTF1 | Forward | gtg cca act ctg tcc taa cta a |
| | Reverse | cta ctg gta ctg tgg taa a |
| DLAT | Forward | ggg tta ttg cac agc gat taa a |
| | Reverse | gaa gaa ttt gct tgc gga act t |
| GAPDH | Forward | act ccc att ctt cca cct ttg |
| | Reverse | ccc tgt tgc tgt agc cat att |

2.9.2 Tissue microarray construction and immunohistochemistry

Tumor and paracancer tissue microarray from Affiliated Tumor Hospital of Nantong University was used for the validation cohort. Primary Anti-FDX1 antibody (1:200; 12592-1-AP, proteintech, China) were applied for the immunohistochemical (IHC) staining. A microscopy system (Nikon, Japan) was used to scan immunohistochemistry sections. We measured the density of positive staining. The H-score was evaluated by two independent pathologists without the knowledge of clinicopathological information.

2.10 Molecular docking

The 3D structures of mitoxantrone were downloaded from PubChem database (<https://pubchem.ncbi.nlm.nih.gov/>). The 3D structure of FDX1 was downloaded from the PDB protein database (<https://www.rcsb.org/>). Further, the protein was dehydrated and ligand extracted. Then, we conduct molecular simulation docking for the mitoxantrone and FDX1.

2.11 Statistical analysis

A complete set of data processing, statistical analysis, and plotting was carried out in R 4.0.3 software. In the case of normally distributed data, the unpaired Student t-test was used, while in the case of non-normally distributed data, the Wilcoxon test was used. An assessment of the correlation between two continuous variables was conducted using Pearson's correlation coefficients. Univariate Cox regression and multivariate Cox regression were used to detect the effect of factors on

prognosis of LUAD,. $P < 0.05$ was regarded as statistically significant.

3 Results

The overall design of this study is displayed in [Figure S1](#).

3.1 Expression of cuproptosis-related genes in carcinoma and adjacent tissues

As described in the literature, 12 genes including FDX1, LIAS, LIPT1, DLD,DLAT, PDHA1, PDHB, MTF1, GLS, CDKN2A, SLC31A1, and ATP7B, were confirmed to be associated with cuproptosis (6). These 12 genes were confirmed in LUAD by comparing their expression patterns in normal and tumor tissues from the TCGA and GTEx databases. It turned out that the expression of these 12 genes was significantly different in both tumor tissues and normal tissues ([Figures 1A, B](#)). Kaplan-Meier plotter shows 9 genes associated with lung adenocarcinoma prognosis and screened for subsequent analysis ([Figure S2](#)). Co-expression analysis combined with prognosis value indicated that the expression of 4 cuproptosis-related genes (PDHB, DLAT, PDHB, DLD) was positively co-expressed with each other, and 9 genes (FDX1, LIPT1, DLAT, PDHA1, PDHB, MTF1, GLS, CDKN2A and SLC31A1) had prognostic value in LUAD ([Figure 1C](#)). Thereafter, we found a significant correlation between the expression of 12 cuproptosis-related genes in the TCGA cohort of LUAD patients ([Figure 1D](#)). The protein-protein interactions network among the cuproptosis-associated genes were displayed in [Figure 1E](#). In parallel, we mapped the

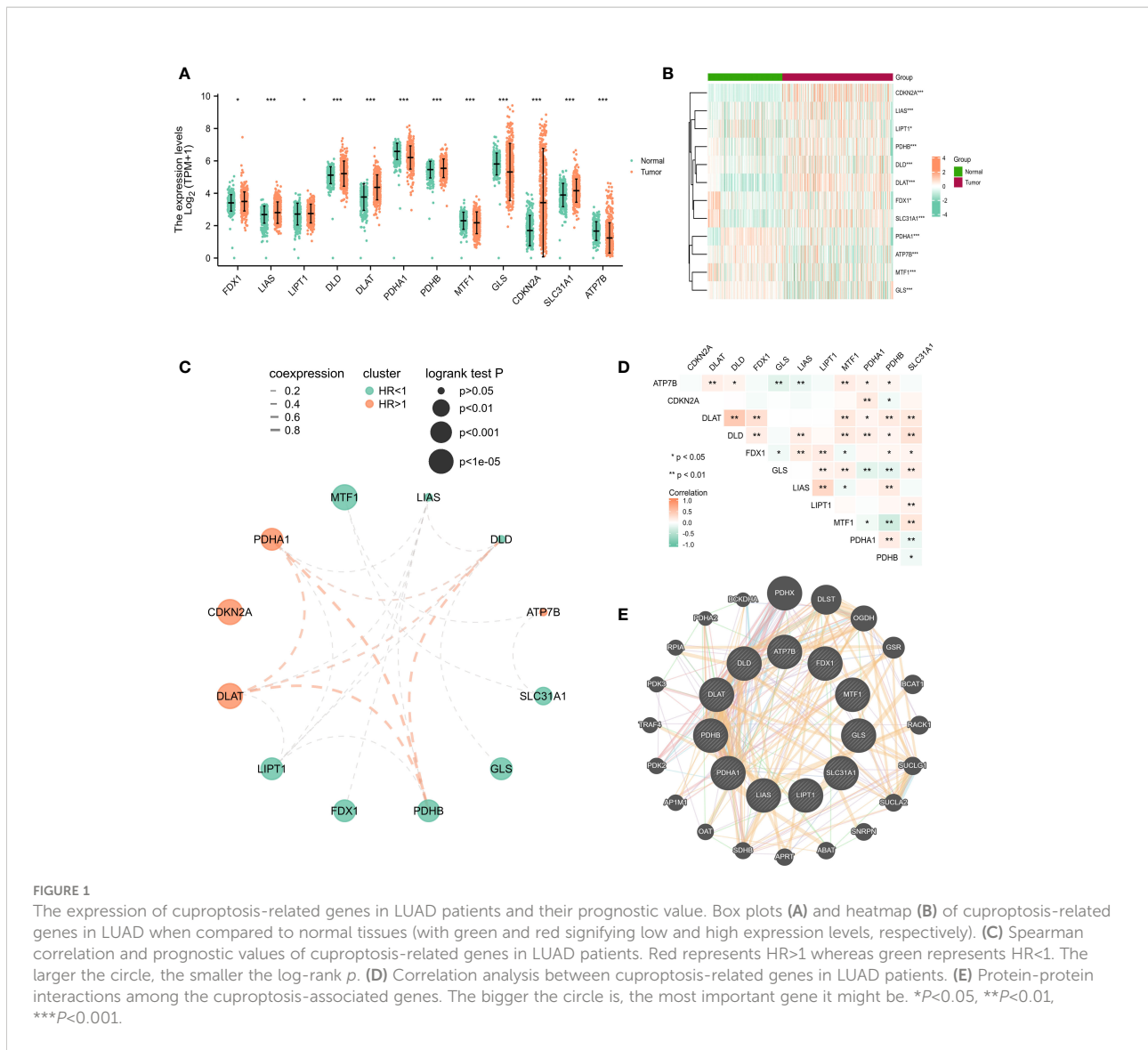


FIGURE 1

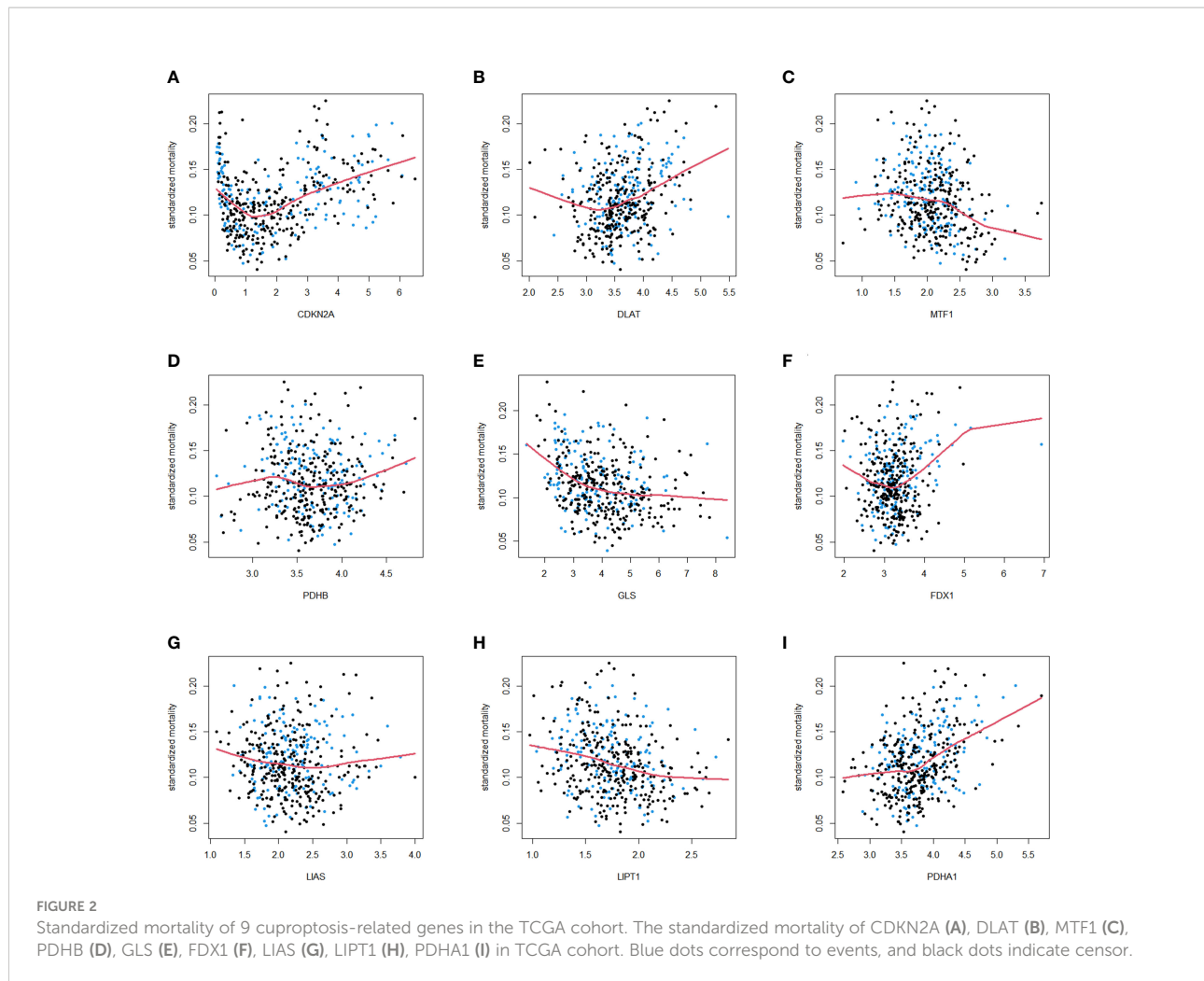
The expression of cuproptosis-related genes in LUAD patients and their prognostic value. Box plots (A) and heatmap (B) of cuproptosis-related genes in LUAD when compared to normal tissues (with green and red signifying low and high expression levels, respectively). (C) Spearman correlation and prognostic values of cuproptosis-related genes in LUAD patients. Red represents HR>1 whereas green represents HR<1. The larger the circle, the smaller the log-rank p. (D) Correlation analysis between cuproptosis-related genes in LUAD patients. (E) Protein-protein interactions among the cuproptosis-associated genes. The bigger the circle is, the most important gene it might be. *P<0.05, **P<0.01, ***P<0.001.

association of prognosis-related genes in the TCGA cohort with the standardized mortality rates (Figure 2).

3.2 Consensus clustering analysis of prognostic cuproptosis-related genes

In a consensus clustering analysis of 442 tumor specimens from the TCGA cohort, 9 cuproptosis-associated genes were compared to the expression of LUAD subtypes to investigate the relationship between the two. Based on the cumulative distribution function curves of the consensus score matrix (CDF) (Figure 3A) and the proportion of ambiguous clustering statistics (PAC) (Figures 3B, C), k=2 was the optimal number. When a pair of samples has a high consensus score, they are more inclined to be clustered into the same

cluster in successive iterations. Consequently, the 442 patients were divided into cluster 1 (n = 288) and cluster 2 (n = 154). Subsequently, a significant difference in OS was observed between patients in two clusters (Figure 3D). The expression of CDKN2A, MTF1, PDHA1, PDHB, SLC31A1 was significantly different between clusters 1 and 2 (Figure 3F). The distribution patterns from PCA analysis showed that samples could completely be distinguished into cluster1 and cluster 2 (Figure 3H). The heatmap showed the relationship between the different expression of genes and clinical characters (Figure 3E), and the volcano plot showed the logFC and FDR value among these genes (Figure 3G). There were 169 upregulated genes as well as 137 downregulated genes between the two clusters. The GSEA enrichment analysis found different expressed genes of the two cluster were enriched in some pathways, including signaling of antigen processing



presentation mediated by class I MHC, transcription regulation of TP53, signaling of B cell receptor BCR and so on (Figure 3J). In addition, the GO enrichment analysis of these genes showed that they were also enriched in certain molecular processes, including histone-serine phosphorylation, response to decreased oxygen levels, multivesicular body, CXCR chemokine receptor binding, etc. (Figure 3I).

3.3 Establishment, evaluation and validation of prognostic signature based on PCRG in TCGA-LUAD

A prognostic model was constructed based on cuproptosis-related genes. In Cox univariate analysis, nine genes associated with cuproptosis were found to be significantly associated with overall survival (OS) in LUAD patients. Eight cuproptosis-related genes were tested and screened out by LASSO analysis (Figures 4A, B). Five genes were extracted using stepwise regression to construct the model (Figure 4C). In order to

develop a risk-score model, the following algorithm was used: Risk score = (0.659854097) * DLAT + (-0.204720564) * GLS + (-0.67817864) * MTF1 + (0.423421209) * PDHA1 + (-0.805217147) * PDHB. The coefficients of the five PCRGs were displayed in Figure 4D, and TCGA-LUAD patients was divided into high-risk score (n = 221) and low-risk score (n = 221) subgroups according to the median to facilitate the next step of study. As a measure of the signature's specificity and sensitivity, areas under curve (AUC) values were calculated for 1-, 3- and 5 years. They were 0.71, 0.68 and 0.63 in TCGA-training set (Figure 4E). In addition, we found that the signature had not only a prognostic value but also a good diagnostic value (Figure 4F, AUC=0.899). We detected the mRNA expression of cuproptosis-related signature in TCGA paired samples and found the expression of DLAT, PDHB, PDHA1 were significantly increased in cancer tissues when compared with cancer-adjacent tissues, while the expression of GLS and MTF1 trended downward, the decrease was not significant between paracancerous tissues and cancer tissues (Figure 4G). In the Human Protein Atlas database, the expressions of GLS, MTF1

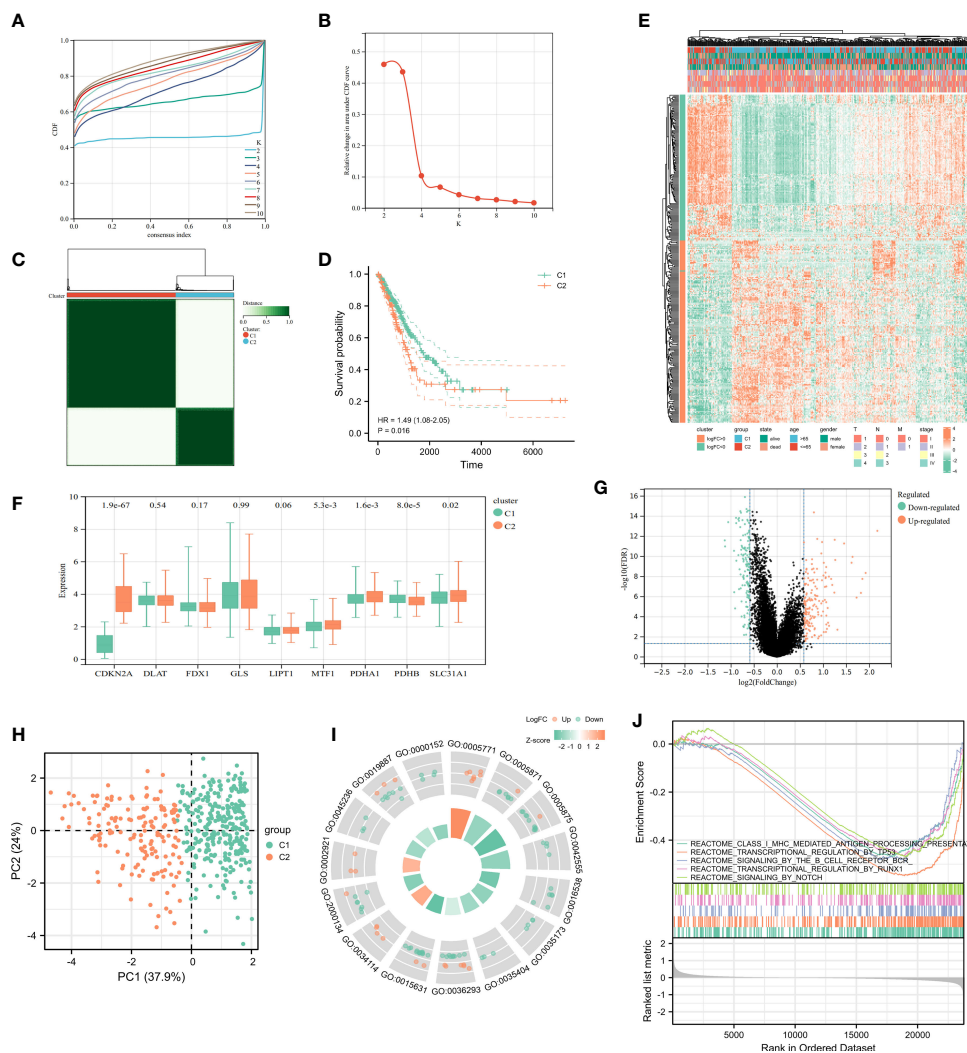


FIGURE 3

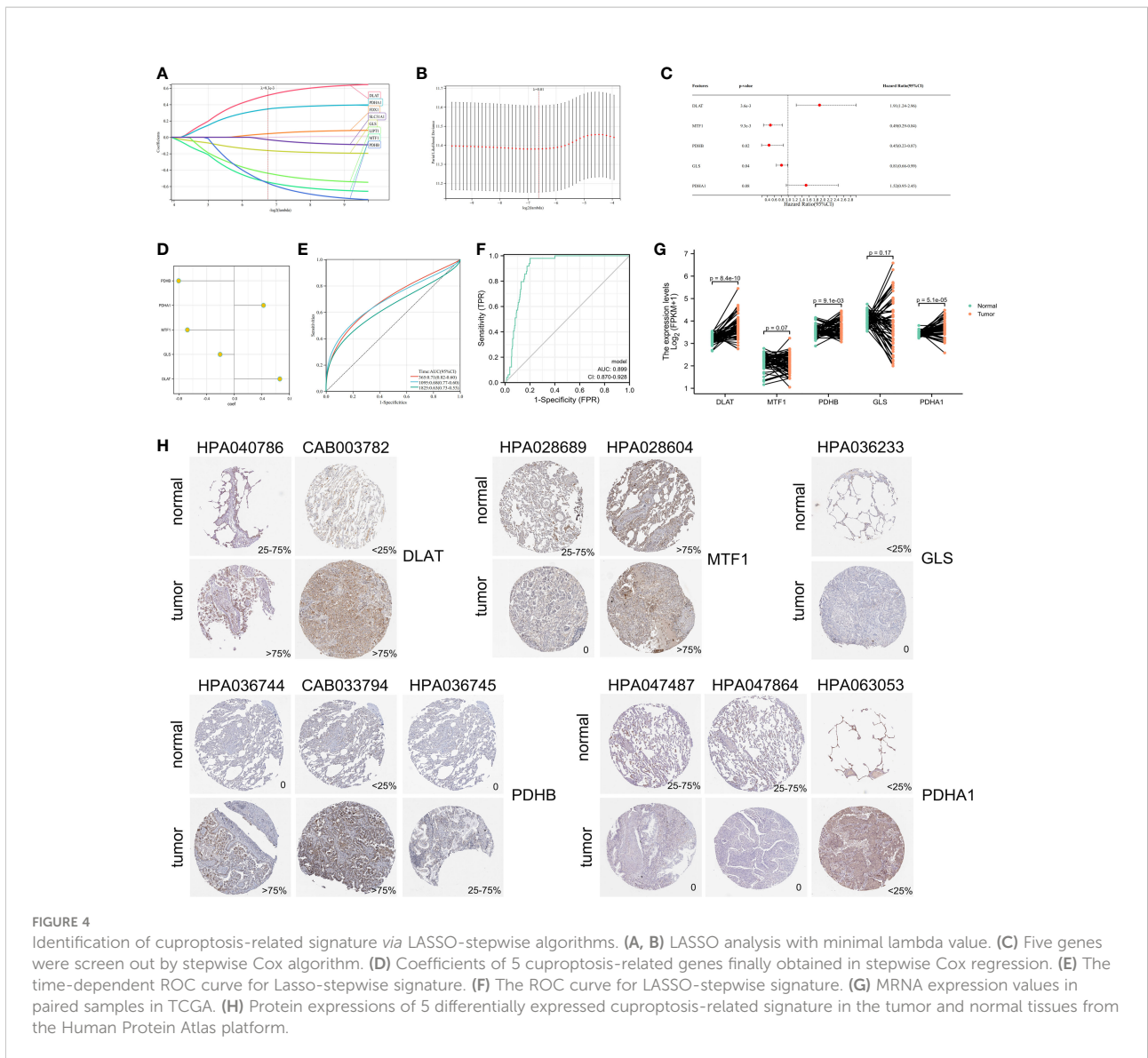
Characteristics of Cuproptosis-related Cluster in TCGA-LUAD cohort. (A) Delta area curve of consensus clustering indicated the relative change in area under the cumulative distribution function (CDF) curve from $k = 2$ to 10. (B) The intragroup correlations were the highest and the intergroup correlations were low when $k = 2$. (C) Cluster diagram for consensus clustering analysis ($k = 2$) of cuproptosis-related genes in 442 LUAD samples in TCGA. (D) Kaplan-Meier curve showed survival probability of cluster1 and cluster2. (E) The heatmap showed the relationship between clinical features and the expression of cuproptosis-related genes in two clusters. (F) The expression of 9 cuproptosis-related genes in two clusters. (G) The volcano plot showed the different expression of genes between the two clusters. (H) PCA analysis for the two clusters. The most significant GO enrichment (I) and multiple pathways by GSEA enrichment analysis (J) in two clusters.

and PDHA1 in tumor tissues were lower compared with those in normal tissues, while the expressions of DLAT and PDHB were significantly higher in tumor tissues compared with those in normal tissues (Figure 4H). Notably, all antibodies in the database were used for each gene to avoid false positives.

The risk survival status charts and Kaplan-Meier (K-M) survival analysis showed that survival time of LUAD patients in the low-risk group was longer than that of LUAD patients in the high-risk group, not only in TCGA training set (Figures 5A, E), but also in TCGA internal testing set (Figures 5B, F) and external verification set (GSE31210 and GSE30219) (Figures 5C, D, G, H).

3.4 Distribution of prognostic riskscores and prognosis stratified by clinical characteristics

According to K-M curves, the OS of the high-risk set was significantly worse than that of the low-risk group in age > 65 subgroups. In clinical subgroups of age ≤ 65 , prognosis was not significant after riskscore stratification (Figure 6A). After stratifying for the characteristic variable of gender, it was found that the OS of the high-risk set was worse than that of the low-risk set in gender subgroups of patients (Figure 6B). In



addition, stratification of pathological staging yielded result that the OS of the high-set was significantly worse than that of the low-risk set in stages III and IV subgroup (Figure 6C). Even though there were no significant difference in the OS of low and high risk sets in age ≤ 65, female, stage I and II subgroups, its overall OS trend was consistent with that seen before stratification. We speculated that this might be due to the lower sample size after stratifying samples and resulting in less statistical power.

Ultimately, even in different clinical subgroups, LUAD patients in the high-risk group had a lower survival probability than those in the low-risk group. In the subgroups after K-means clustering, it showed a significant difference in the distribution of riskscore, which proved the consistency of K-means clustering resulted with cuproptosis-related signature results (Figures 5E-H). Combining the analysis results of the K-means algorithm, we

found that the riskscore was higher in Cluster 2 compared to the Cluster 1 (Figure 6D). The distribution of riskscores differed significantly between survival outcomes, suggesting that those who occurring ending events were more likely to be from a high-risk group (Figure 6E). There was no significant difference in the distribution of the riskscore between the two subgroups (aged > 65 years or ≤ 65 years), implying that age was not a factor affecting the distribution of the riskscore (Figure 6F). However, gender affected the distribution of the riskscore, with female patients having lower riskscore values compared to male patients (Figure 6G). It was noteworthy that the riskscores were higher as the tumor development and pathological stage changed (Figure 6H). The above results suggest that after stratification of clinical features, our riskscore distribution influenced prognostic outcomes, and our signature has high specificity and sensitivity in predicting the prognosis of LUAD patients.

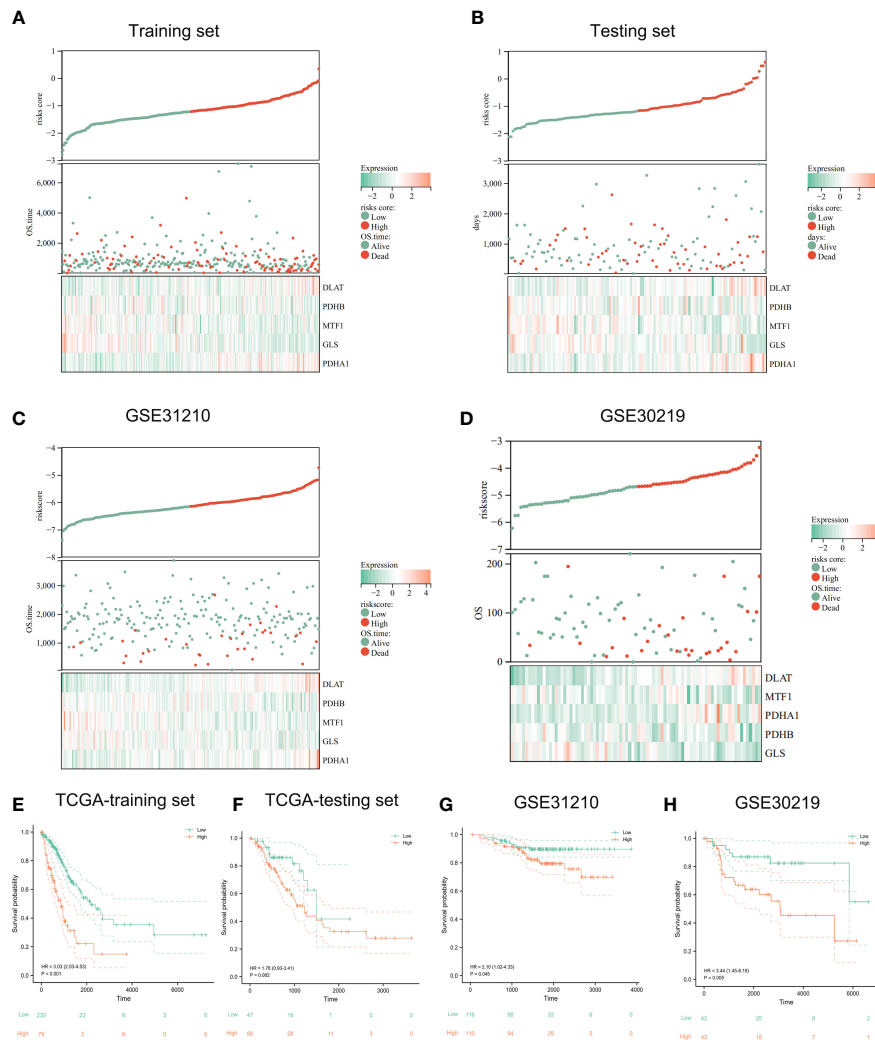
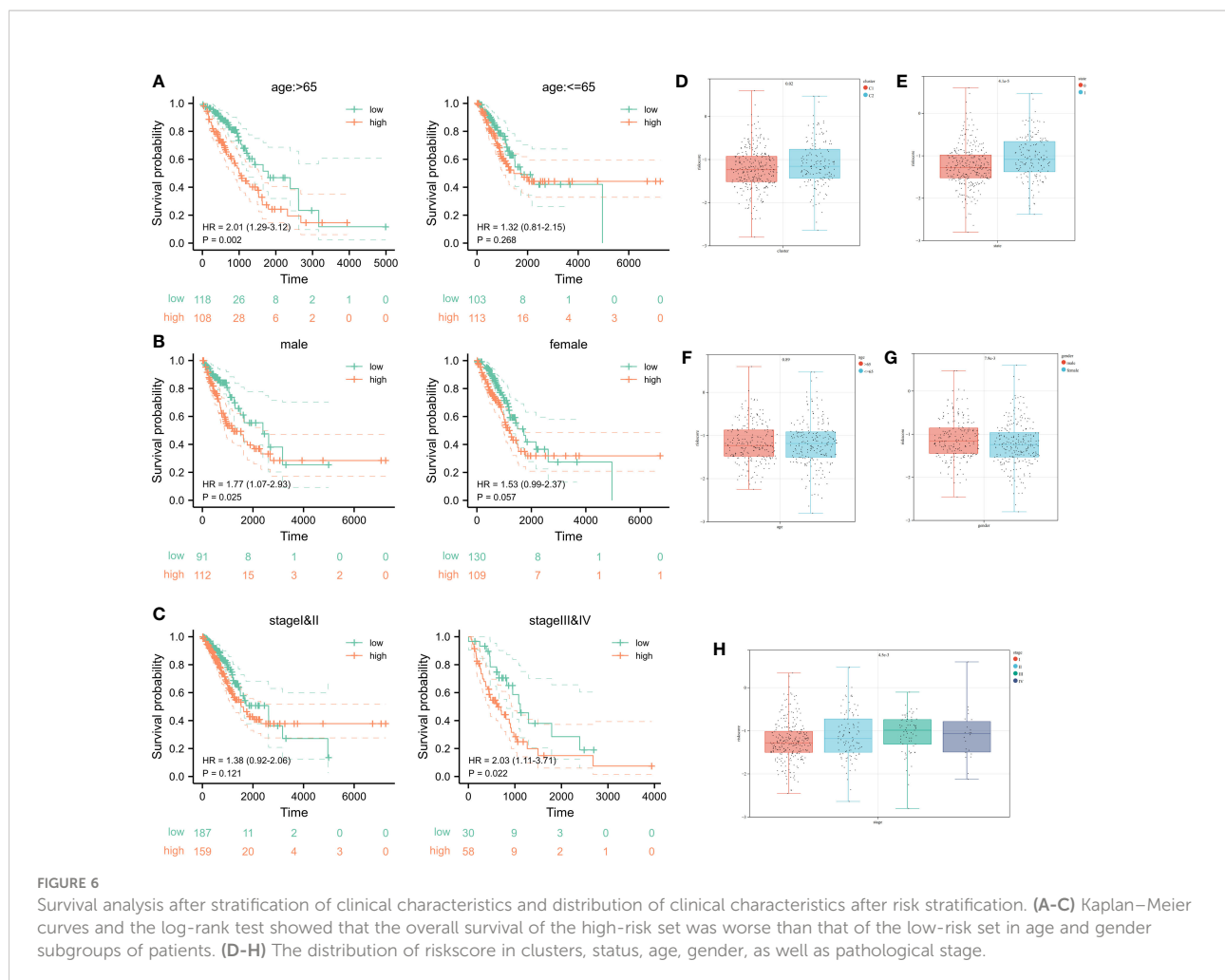


FIGURE 5 Evaluation and validation of prognostic signature. The risk-score, survival time, survival status and gene expression of the training set (A), testing set (B), and external set GSE31210 (C) and GSE30219 (D). Kaplan-Meier analysis demonstrated the prognostic significance of the risk model in TCGA training set (E), testing set (F) and GSE31210 (G), GSE30219 cohort (H).

3.5 Identification of cuproptosis-related modules derived from riskscore patterns

Setting the soft threshold β to 7 (unsigned, $R = 0.86$) in the WGCNA could provide a suitable power value for the co-expression network (Figures 7A, B). After identifying 8 different modules, the correlation between different color modules and clinical features was calculated separately (Figures 7C, D). Brown module and riskscore subgroups exhibited the highest correlation of module-trait relationships. For the brown module, the R value between GS and MM was reached 0.74 in riskscore (Figure 7E) and 0.44 in status (Figure 7F), which suggested that the cuproptosis-related module was well constructed and the module was significantly associated with prognosis. To identify Hub

cuproptosis-related module derived from cuproptosis-related patterns within the brown module, 167 genes with $GS > 0.7$ and $MM > 0.2$ were considered hub cuproptosis-related genes. The GO analysis of these hub genes was enriched into the lymphocyte differentiation, T cell activation, lymphocyte proliferation, protein complex involved in cell adhesion, inflammasome complex, immunological synapse, guanyl-nucleotide exchange factor activity, GTPase regulator activity and so on (Figure 7G). KEGG analysis enriched these genes into Chemokine signaling pathway, B cell receptor signaling pathway, PD-L1 expression and PD-1 checkpoint pathway in cancer and so on (Figure 7H). This suggested that our modules closely related to the cuproptosis-related signature and mainly affected the immunomodulation of patients with LUAD.



3.6 Immune infiltration analysis for cuproptosis-signature

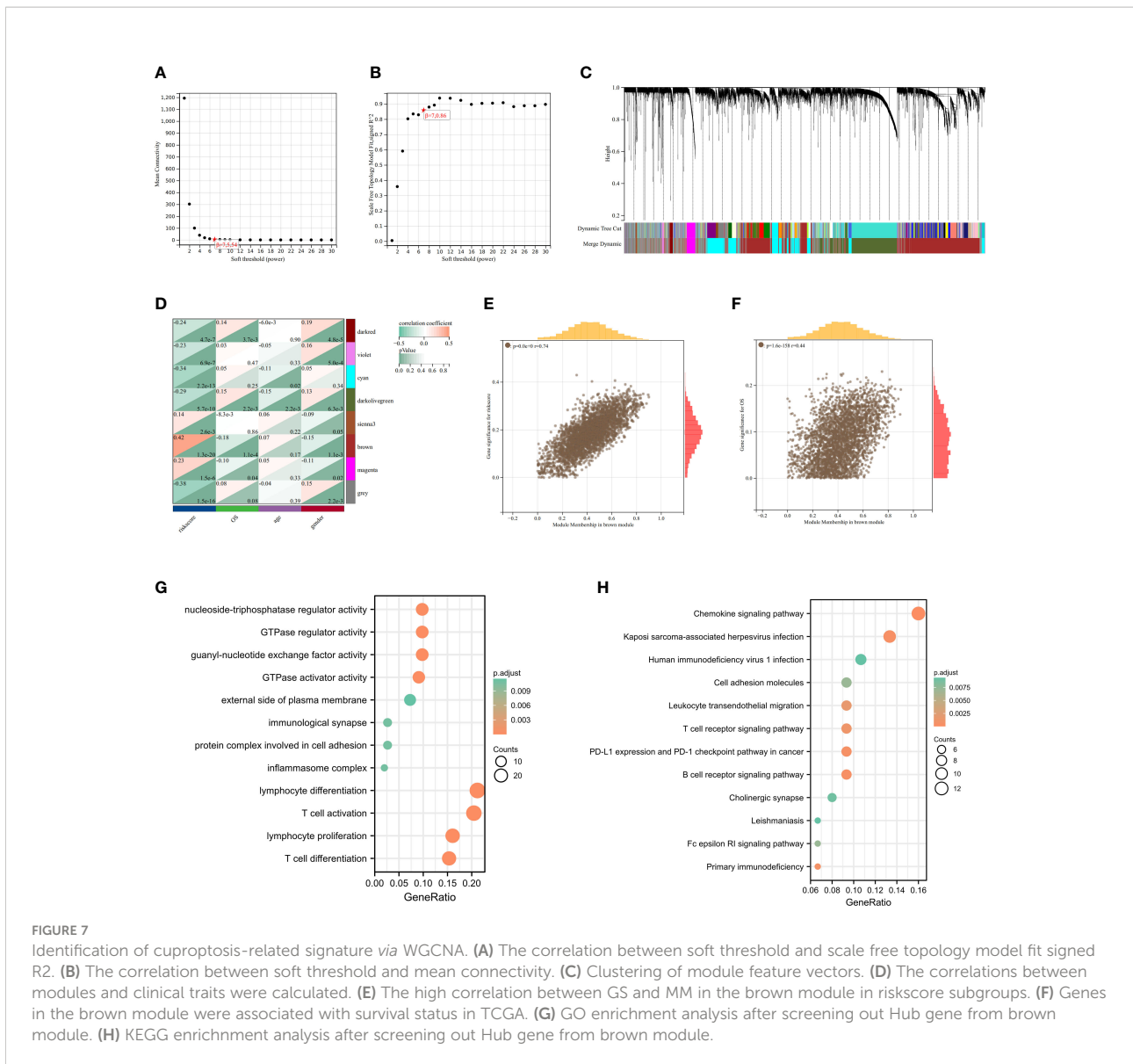
The heatmap showed the relationship between the riskscore subgroups and clinical characters (Figure 8A). The volcano plot showed the logFC and FDR value among these different expressed genes (Figure 8B).

As part of this study, we performed enrichment analyses on GO (Figure 8C), GSEA (Figure 8D), and GSVA (Figure 8E) to elucidate the underlying functions and pathways associated with our prognostic features. The results of GO, GSEA, GSVA, and WGCNA all suggested that genes associated with our prognostic features were associated with immune infiltration. Meanwhile, Riskscores were negatively correlated with CD274 (PD-L1) and CTLA4 expression (Figure 9A). We evaluated the differences in infiltration of 22 immune cell types in the riskscore subgroup through the Cibersort database (Figures 9B, C). The results showed that B cells naive, Plasma cells, etc. were significantly higher while T cells CD4 memory resting, Macrophages M2, mast cells resting were significantly lower in the high-risk group when compared to the low-risk group. To demonstrate that the functions of the two

subgroups were not biased by the analytical algorithm, Xcell (Figure 9D), ESTIMATE (Figures 9E–H), and MCP-counter (Figure 9I) algorithms were used to verify the stability and robustness of the Cibersort result. We further found significant differences in common immune checkpoints between the two subgroups as well (Figure 9J). HLA genes are also closely related to tumor immunity (16). Additionally, we examined whether HLA-related genes were expressed differently in risk subgroups. High-risk individuals tended to have lower HLA gene expression than low-risk individuals (Figure 9K). Together, these results revealed a higher tumor purity with lower immune cell infiltration in high-risk subgroup, which may affect immunotherapy outcomes in LUAD patients.

3.7 Clinical applications for cuproptosis-signature

Identification of 20 important small molecules through the L1000FWD database as drugs to improve poor prognosis in high-risk groups (Figure 10A). Mitoxantrone was predicted to be



the most promising drug. We further visualized the 2D (Figure 10B) and 3D (Figure 10C) structure of Mitoxantrone. A nomogram was created by integrating clinical information and genetic features from TCGA and performing multivariate Cox regression models (Figure 10D). Calibration plots were applied in OS outcomes, which demonstrated favorable concordance between predicted and observed OS at 1-, 3- and 5-year survival (Figure 10E). In terms of prediction, the C-index was 0.70 (0.67-0.73), which reflects relatively good performance. Also, LUAD-patients with high score had worse survival than those with low score (Figure 10F). The AUC values of 1-, 3- and 5-year in nomogram were 0.72, 0.74 and 0.74, respectively (Figure 10G). Additionally, we evaluated the nomogram model in TCGA-LUAD using decision curve analysis (DCA) (Figure 10H). Altogether, risk score was an independent and good

prognostic indicator, and LUAD patients could benefit more after combining with pathological stage, T-stage and risk scores.

3.8 Validation of *in vitro* experiments and molecular docking

To confirm the role of cuproptosis-signature in LUAD, we further verified their differential expression in normal and tumor samples by *in vitro* experiments. qRT-PCR was performed in paired samples of cancer and paracancer to detect mRNA expression levels of the prognostic cuproptosis-signature. We found that the expression of PDHA1, GLS, DLAT, PDHB and MTF1 were differed between cancer and paracancer (Figure 11A). We have deciphered that the small molecule

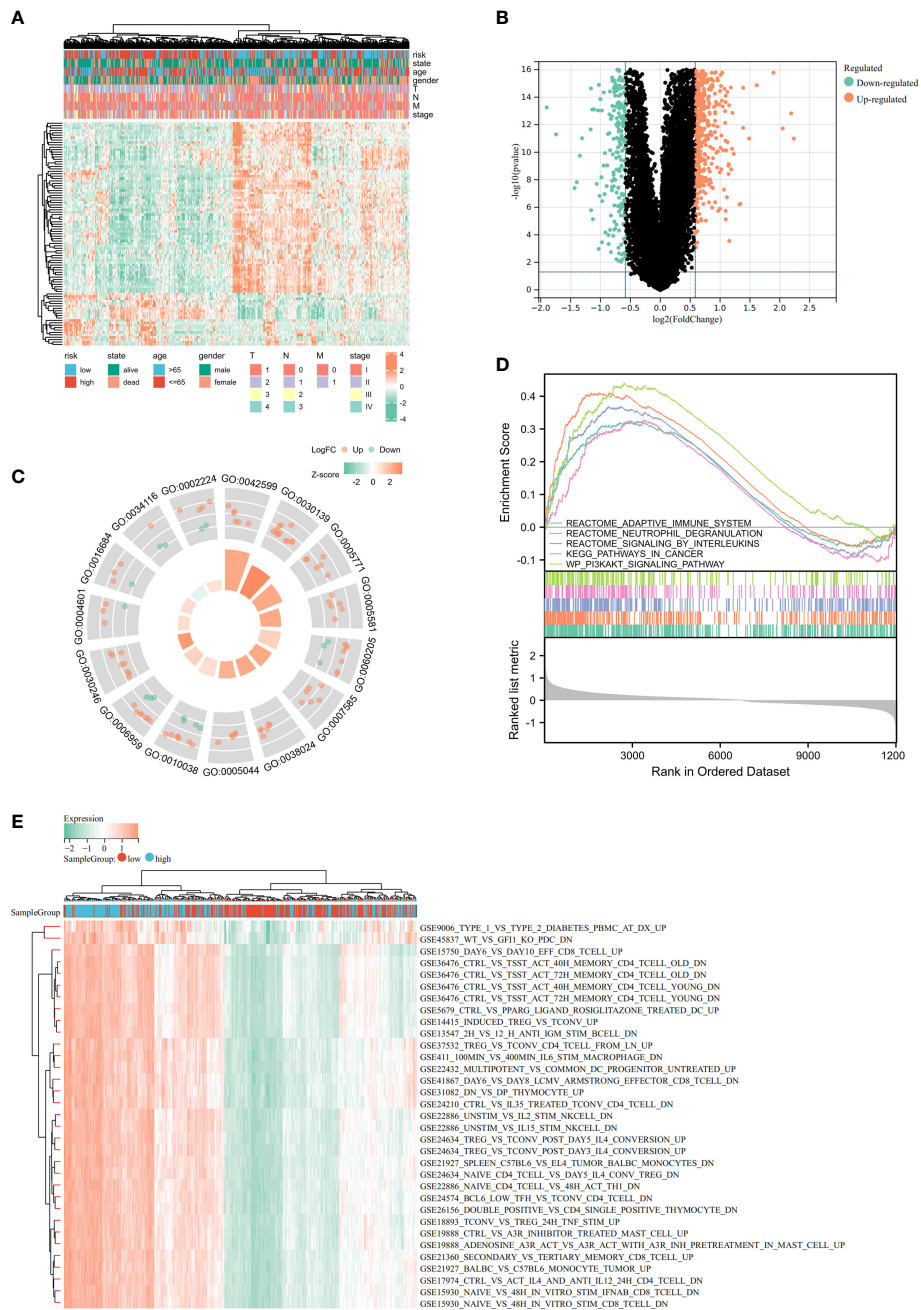
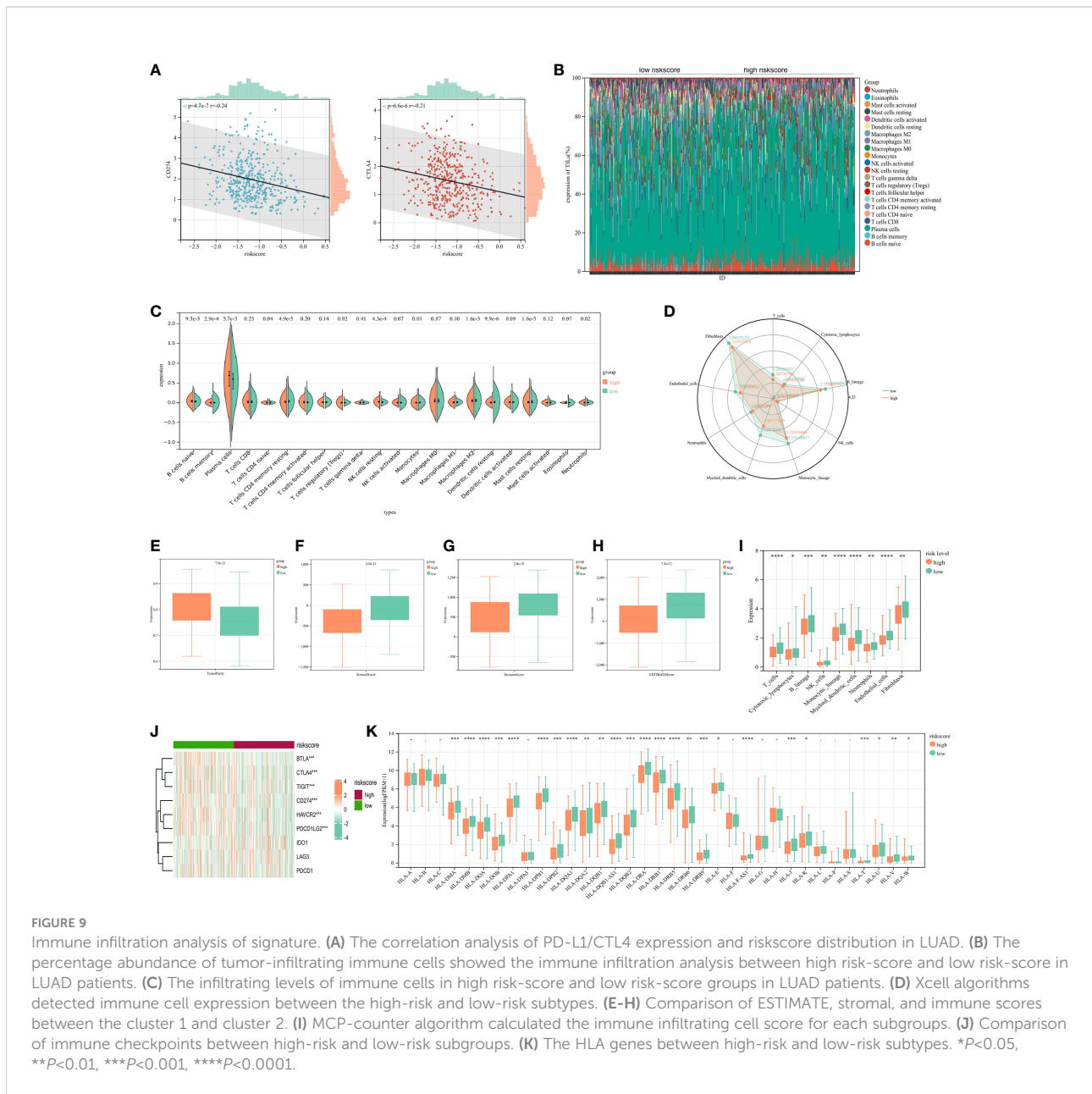


FIGURE 8 Identification of differentially expressed genes (DEGs) and potential signaling pathways in different isoforms. The heatmap (A) and volcano plot (B) of the differential gene expression between high and low expressed cuproptosis-related signature in LUAD. GO enrichment (C) and GSEA (D) analysis of the differential expressed genes. (E) GSEA enrichment analysis of the differential genes.

compound mitoxantrone could treat the risk of death due to immune tolerance induced by cuproptosis-related signature. FDX1 as an enzyme catalyzing cuproptosis-related signature (17), we further used molecular docking to verify the direct interaction of FDX1 with the small molecule compound mitoxantrone (Figure 11B).

Next, tissue microarray of 301 lung cancer patients from the Nantong Cancer Hospital were used in a cohort study. FDX1 expression was identified by immunohistochemical staining in 301 lung cancer samples. We observed that FDX1 was located in the cytoplasm of tumor cells (Figure 11C). Immunohistochemical score (H-score) for immunostaining of tumor tissues also differed



in each sample (Figure 11D). 119 (39.5%) patients were classified into FDX1 low expression subgroup while the FDX1 high expression subgroup had 182 (60.5%) patients. In our cohort, the patients with high FDX1 expression had significantly better outcomes than those with low FDX1 expression (Figure 11E). Stratification by pathological type revealed that the high expression group of FDX1 had a better prognosis than the low expression group in both LUAD and other lung cancer patients (Figures 11F, G). Most importantly, we constructed Nomogram and found that H-score was one of the most significant independent predictors of OS (Figure 11H). The Harrell's *c*-index for the nomogram model to predict the overall survival was 0.81. In a word, our study showed that FDX1, a key enzyme for

cuproptosis, affected the prognosis of lung cancer patients by influencing the expression of GLS, PDHA1, PDHB, DLAT, and MTF1.

4 Discussion

Globally, lung cancer is the leading cause of death among cancer patients. Approximately 40% of all the diagnosed cases were LUADs (2). Immune escape and drug resistance are the major drivers of cancer death and begin when cancer cells invade surrounding tissues. With the recent advent of molecularly targeted therapies and immunotherapies, survival in LUAD

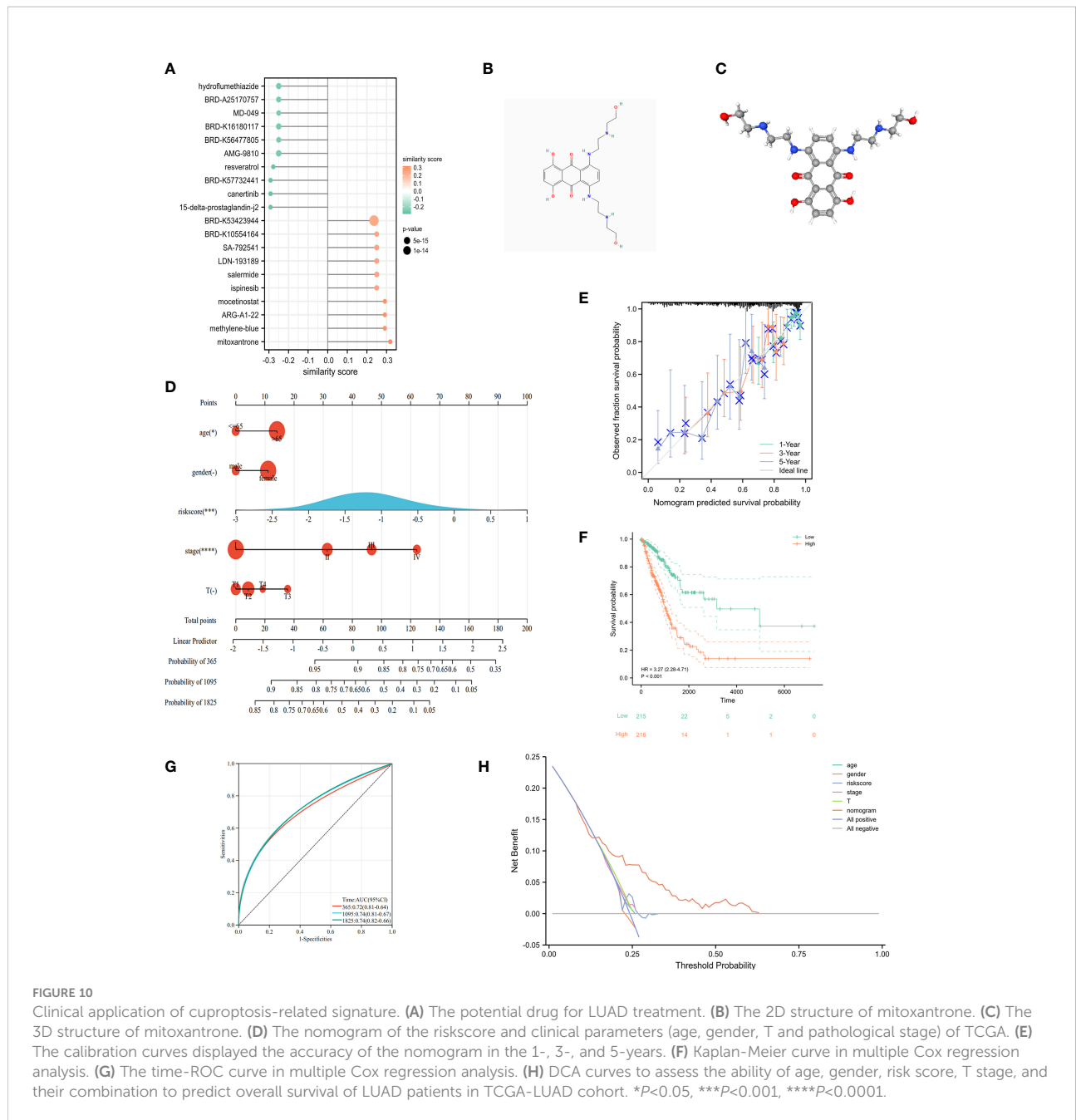


FIGURE 10

Clinical application of cuproptosis-related signature. (A) The potential drug for LUAD treatment. (B) The 2D structure of mitoxantrone. (C) The 3D structure of mitoxantrone. (D) The nomogram of the riskscore and clinical parameters (age, gender, T and pathological stage) of TCGA. (E) The calibration curves displayed the accuracy of the nomogram in the 1-, 3-, and 5-years. (F) Kaplan-Meier curve in multiple Cox regression analysis. (G) The time-ROC curve in multiple Cox regression analysis. (H) DCA curves to assess the ability of age, gender, risk score, T stage, and their combination to predict overall survival of LUAD patients in TCGA-LUAD cohort. * $P < 0.05$, *** $P < 0.001$, **** $P < 0.0001$.

has been highly improved. However, drug resistance and recurrence remain the main causes of tumor progression in patients with LUAD and are influenced by factors inherent to immune cells, cancer cells, or both (18). The immune escape and resisting tumor cell death are hallmarks of cancer as well as the basis for acquiring resistance following immunotherapy (19, 20). New discoveries of programmed cell death patterns and the elucidation of related molecular mechanisms continually update our knowledge of cell death in tumors. Recently, a new form of cell death with copper-dependence, called cuproptosis, was first proposed by Tsvetkov et al (17). There have been several studies

showing an association between copper metabolism and tumorigenesis, as well as a higher copper demand by cancer cells than by normal cells, and that dysregulation of copper ions is significantly associated with drug resistance (21). Liao et al. considered that copper metabolism might be responsible for the development of colorectal cancer with an immune response (7). Currently, the specific mechanism of cuproptosis-related genes in LUAD remains unclear.

In our study, we first found that 8 cuproptosis-related genes were upregulated, while 4 genes were downregulated in LUAD when compared to normal tissues. Then, the K-means algorithm divided

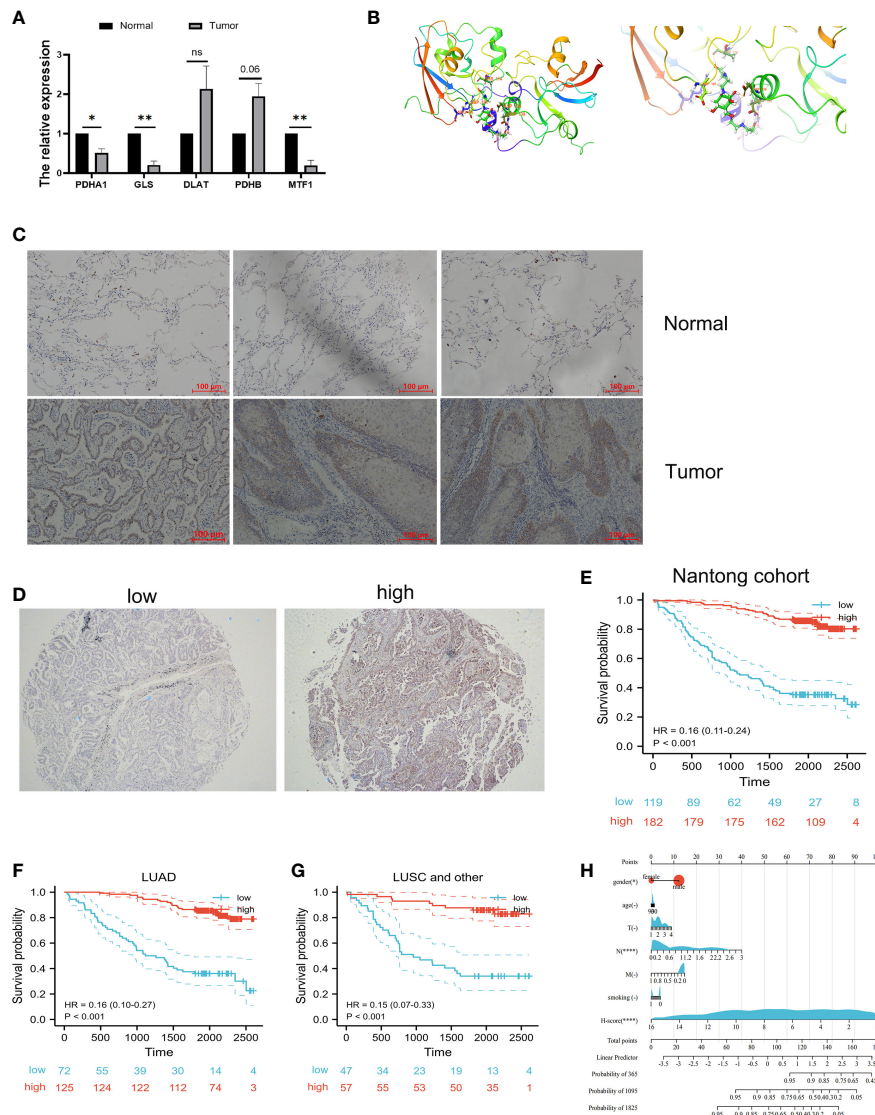


FIGURE 11 Validation of *in vitro* experiment and molecular docking. **(A)** Validation of mRNA expression in prognostic cuproptosis-related signature by qRT-PCR. * $P < 0.05$, ** $P < 0.01$. **(B)** The molecular docking between FDX1 and mitoxantrone. **(C)** The IHC results showed that FDX1 protein is highly expressed in tumor tissues when compared with normal tissues. **(D)** Representative immunohistochemical microarray of FDX1. **(E)** Kaplan–Meier curves showed that the overall survival of the low-risk set was worse than that of the high-risk set in Nantong cohort. **(F, G)** Kaplan–Meier curves showed that the overall survival of the low-risk set was worse than that of the high-risk set in LUAD **(F)** and lung squamous cell (LUSC) subgroups **(G)** of patients. **(H)** The nomogram of the H-score and clinical parameters (age, gender, smoking and T, N, M stage) of Nantong cohort. ns, not significant.

the cohort into two clusters, and the set of genes associated with cuproptosis in LUAD was mainly enriched in MHC-I mediated antigen processing expression, transcriptional regulation of TP53, and signaling of the B cell receptor BCR in cluster 2, whose OS was obviously poorer than that in cluster 1. These above results suggested that the prognostic differences between cuproptosis-related clusters were associated to immune response. There were five PCRGs derived from univariate regression, LASSO, and stepwise regression. Then after, five PCRGs were used to construct a novel

prognostic risk signature, which stratified LUAD patients into high- and low-risk subgroups. Differential cuproptosis-related mRNA expression was verified in TCGA paired samples, and protein expression of cuproptosis-related signature was further verified in Human Protein Atlas platform. The prognostic signature integrated 5 PCRGs, including DLAT, MTF1, PDHB, GLS and PDHA1. Among them, DLAT and PDHA1 were associated with poor prognosis of LUAD while MTF1, PDHB and GLS were associated with good prognosis of LUAD.

DLAT (dihydrolipoamide S-acetyltransferase) is expressed in mitochondria which involved in cell glycolysis. A number of malignancies, including lung cancer (22), gastric cancer (23) and colon cancer (24), have been associated with high expression of DLAT in various tumors. These studies suggested a potential role of DLAT in abnormal cuproptosis metabolism in LUAD. Similarly, copper-induced cell death was mediated by protein lipoylation. PDHA1 (pyruvate dehydrogenase E1 subunit alpha 1) as a hub gene in Fatty acid metabolism pathway, played an important role in cuproptosis. Chen et al. found that high expression of PDHA1 in NSCLC promoted tumor progression *in vivo* and *in vitro* (25). Notably, PDHA1 was highly expressed in LUAD by Human Protein Atlas platform analysis, which was opposite of mRNA expression in TCGA, indicating that PDHA1 might not regulated in mRNA level in LUAD. Interestingly, MTF1, PDHB and GLS were reported to be highly expressed in other tumor types, while in our study, we found that these genes were strongly associated with good prognosis. MTF1 (metal regulatory transcription factor 1) responds sensitively to both metal excess and deficiency, protects cells from oxidative and hypoxic stresses (26), is dysregulated in cancer and pain disease (27). As a consequence of the mitochondrial respiratory and functional impairment in LUAD, cells lacking MTF1 are more sensitive to oxidative stress. PDHB (pyruvate dehydrogenase E1 subunit beta) encodes a subunit of the pyruvate dehydrogenase complex, which converts pyruvate to acetyl-CoA in the mitochondrion (28). Zhu et al. found that PDHB was associated with tumor growth and metastasis and glycolysis (29). GLS (glutaminase) is oncogenic and can influence the metabolic reprogramming of cancer through its functional selective genome and epigenome (30). A recent study showed that in pancreatic ductal adenocarcinoma (PDAC), activated GLS increased glutamine catabolism and production of nicotinamide adenine dinucleotide phosphate (NADPH) and glutathione, which prevented from being oxidative and promoting tumor cell survival and tumor growth in mice (31). Taken together, all of the five crucial genes were involved in tumorigenesis and progression by regulating pathways associated with tumor metabolism. Additionally, our data further elucidated the important role of these 5 PCRGs in LUAD, and the PCRGs for LUAD patients were highly sensitive and specific.

Immunotherapy has been a powerful clinical strategy for treating cancer (32). PD-1/PD-L1 checkpoint blockade immunotherapy has joined chemotherapy as a standard treatment for lung cancer (33). Unfortunately, the metabolic reprogramming of tumors poses a considerable challenge for cells to perform their immune functions as well as to cancer immunotherapy (34). In particular, cells containing high lipid acylated proteins are more sensitive to copper-induced cell death. Thus, in tumors characterized by high lipid metabolism, the induction of copper death in cells may be able to resolve drug resistance caused by immune escape. As expected, our results of

WGCNA algorithm, GO and KEGG analysis were significantly associated with immune response related pathways, including T cell receptor signaling pathway, PD-L1 expression and PD-1 checkpoint pathway in cancer, B cell receptor signaling pathway. Similarly, Limma package further validated that the immune pathways were enriched by cuproptosis-associated genes. Notably, these pathways, such as the adaptive immune system, signaling by GPCR and PI3K/AKT/mTOR signaling have been widely confirmed to be involved in LUAD (35). Taken together, the application of two machine learning algorithms revealed that there was an inextricable connection between copper-dependent cell death and tumor immune responses in LUAD (36).

A major finding of previous study found tumor purity was negatively correlated with immune response and might be a proxy for the level of immune response in the tumor microenvironment (37). Consistent with the finding, in our study, the tumor purity was higher and the immune infiltration was lower in high-risk set when compared with the low-risk one. The abundances of B cells, plasma cells, resting memory T cells CD4, resting NK cells, monocytes, M2 macrophages, resting DCs, resting mast cells, and neutrophils were substantially different between high and low riskscore group. Ample evidence has shown that the infiltration of B cells, especially naive B cells, memory B cells, and plasma cells is associated with a good prognosis of LUAD (38). In contrast, we found the high-risk subgroup had a poor prognosis while high plasma cell expression. It is difficult to explain the discrepancy between these data and our results. Considering the loss of an HLA allele may be a mechanism of immune escape (39), we can only speculate that the decreased expression of HLA genes as well as immune checkpoint genes in the high-riskscore group is likely to be associated with dysregulation of immune cells. More data is needed in the future to support this conjecture.

Afterward, to verify the general applicability of the riskscore subgroups, validation was performed on the internal validation set and the external validation set GSE31210. The signature exhibited good predictive performance for both the internal and external validation sets. ROC curves and Kaplan-Meier curves showed that PCRGs were good predictors of prognosis in LUAD patients. It is worth noting that after stratified analysis of clinical characteristics, the signature still produced significant prognostic differences in the LUAD patients. In other words, the cuproptosis-related signature had good predictive performance in OS and may serve as an independent prognostic indicator for LUAD. Nomogram was constructed to further advance clinical applications and the accuracy of the maps was verified with calibration plots. Small molecule drugs have been now commonly used in the treatment of cancer and widely used in clinical practice (40). Our study identified 20 small molecule drugs that were most significant for LUAD treatment. The top 2 of them were mitoxantrone and 15-delta-prostaglandin-j2. Mitoxantrone has been found to treat breast cancer through blocking cellular autophagy (41). Whether Mitoxantrone can inhibit tumor development by activating

autophagy or copper death in LUAD needs to be further investigated. In addition, 15-delta-prostaglandin-j2 was a natural ligand for PPAR γ . Activation of PPAR γ is well known to be beneficial in the treatment of breast and colon cancers (42). PPAR γ plays a pivotal role in lipid metabolism (43) and protein lipoylation is necessary for copper death. Thus, the role of PPAR γ in LUAD deserves further elucidated.

Functionally, FDX1 catalyzes proteolipidylation of a battery of substrates, as the most prominent marker of cuproptosis. Previous bioinformatic analysis of cuproptosis-related genes is mainly at the plane of RNA transcriptional regulation (44–46), ignoring the fact that the function of proteases depends mainly on protein expression and activity. As far as we know, our study was the first investigation illustrating the correlation between FDX1 protein expression and unfavorable prognosis of lung cancer patients by tissue microarray. FDX1 as the bridge between unfavorable prognosis of lung cancer patients and cuproptosis.

Mechanically, Mo. et al. found that lncRNA MIR31HG/miR-193a-3p/TNFRSF21 axis may indirectly regulates the occurrence of cuproptosis in lung adenocarcinoma. Wang et al. considered lncUCA1/miR-1-3p/DLD axis leading to the occurrence of cuproptosis (47). These studies involve in pre-transcriptional regulation and lack direct favorable evidence for the role of cuproptosis phenomenon in the prognostic outcome of lung adenocarcinoma patients. Chen et al. discovered the alterations in mRNAs such as BARX1, ENTP2 were found to be associated with the influence of elesclomol (48). These experiments on these cells lines only indirectly demonstrate the occurrence of possible cuproptosis-related mRNA alterations at the cellular level. We constructed a cuproptosis-related signature by bioinformatic analysis, in which five genes serve as direct substrates of FDX1 and their alterations are the most significant markers of cuproptosis. FDX1 affects the prognosis of lung cancer by altering the expression of cuproptosis-related signature (GLS, PDHA1, PDHB, MTF1, and DLAT), which more strongly confirms that the prognosis of lung cancer patients is closely related to the occurrence of cuproptosis.

Several limitations are worth mentioning. Sincerely, the hypothesis needs to be further validated by more research. To begin with, the study only included cohorts from TCGA, GEO and Nantong cohort. It is not possible to fully assess the quality of the data, to further evaluate the prognostic cuproptosis-signature in the future, a prospective, multicenter study is required. Lastly, to further clarify the mechanism and function of the cuproptosis-signature in tumorigenesis and LUAD progression, *in vivo* experiment might be conducted.

In conclusion, the purpose of this research was to develop a prognostic cuproptosis-related signature, which could be used to predict survival of LUAD patients, reflecting the tumor immune infiltration. What's more, it may be a key to improve the prognosis for LUAD patients through immunotherapy. It is expected that this research will provide new insights into how to diagnose and treat LUAD patients with precision.

Data availability statement

The datasets presented in this study can be found in online repositories. The names of the repository/repositories and accession number(s) can be found in the article/Supplementary Material.

Ethics statement

The studies involving human participants were reviewed and approved by the ethics committee of the Affiliated Tumor Hospital of Nantong University. The patients/participants provided their written informed consent to participate in this study.

Author contributions

A formal analysis was conducted and the initial draft was written by YL. The article was written, reviewed, and edited by WL, YY, JS, GW, and HZ contributed to the conception of this research. AS supervised all experiments. All authors contributed to the article and approved the submitted version.

Funding

This study was supported by the Nantong Municipal Health Commission scientific research project (QA2021028 and MSZ21037).

Conflict of interest

The authors declare that the research was conducted in the absence of any commercial or financial relationships that could be construed as a potential conflict of interest.

Publisher's note

All claims expressed in this article are solely those of the authors and do not necessarily represent those of their affiliated organizations, or those of the publisher, the editors and the reviewers. Any product that may be evaluated in this article, or claim that may be made by its manufacturer, is not guaranteed or endorsed by the publisher.

Supplementary material

The Supplementary Material for this article can be found online at: <https://www.frontiersin.org/articles/10.3389/fonc.2022.1080985/full#supplementary-material>

References

- Ganti AK, Klein AB, Cotarla I, Seal B, Chou E. Update of incidence, prevalence, survival, and initial treatment in patients with non-small cell lung cancer in the US. *JAMA Oncol* (2021) 7:1824–32. doi: 10.1001/jamaoncol.2021.4932
- Kim N, Kim HK, Lee K, Hong Y, Cho JH, Choi JW, et al. Single-cell RNA sequencing demonstrates the molecular and cellular reprogramming of metastatic lung adenocarcinoma. *Nat Commun* (2020) 11:2285. doi: 10.1038/s41467-020-16164-1
- Lin JJ, Chin E, Yeap BY, Ferris LA, Kamesan V, Lennes IT, et al. Increased hepatotoxicity associated with sequential immune checkpoint inhibitor and crizotinib therapy in patients with non-small cell lung cancer. *J Thorac Oncol* (2019) 14:135–40. doi: 10.1016/j.jtho.2018.09.001
- Zuo S, Wei M, Zhang H, Chen A, Wu J, Wei J, et al. A robust six-gene prognostic signature for prediction of both disease-free and overall survival in non-small cell lung cancer. *J Transl Med* (2019) 17:152. doi: 10.1186/s12967-019-1899-y
- Voss J, Ford CA, Petrova S, Melville L, Paterson M, Pound JD, et al. Modulation of macrophage antitumor potential by apoptotic lymphoma cells. *Cell Death Differ* (2017) 24:971–83. doi: 10.1038/cdd.2016.132
- Tang D, Chen X, Kroemer G. Cuproptosis: a copper-triggered modality of mitochondrial cell death. *Cell Res* (2022) 32:417–8. doi: 10.1038/s41422-022-00653-7
- Liao Y, Zhao J, Bulek K, Tang F, Chen X, Cai G, et al. Inflammation mobilizes copper metabolism to promote colon tumorigenesis via an IL-17-STEAP4-XIAP axis. *Nat Commun* (2020) 11:900. doi: 10.1038/s41467-020-14698-y
- Zheng P, Zhou C, Lu L, Liu B, Ding Y. Elesclomol: a copper ionophore targeting mitochondrial metabolism for cancer therapy. *J Exp Clin Cancer Res* (2022) 41:271. doi: 10.1186/s13046-022-02485-0
- Carneiro BA, El-Deiry WS. Targeting apoptosis in cancer therapy. *Nat Rev Clin Oncol* (2020) 17:395–417. doi: 10.1038/s41571-020-0341-y
- Li G, Luo Q, Wang X, Zeng F, Feng G, Che G. Deep learning reveals cuproptosis features assist in predict prognosis and guide immunotherapy in lung adenocarcinoma. *Front Endocrinol (Lausanne)* (2022) 13:970269. doi: 10.3389/fendo.2022.970269
- Tang Y, Li Q, Zhang D, Ma Z, Yang J, Cui Y, et al. Cuproptosis-related gene signature correlates with the tumor immune features and predicts the prognosis of early-stage lung adenocarcinoma patients. *Front Genet* (2022) 13:977156. doi: 10.3389/fgene.2022.977156
- Wu M, Bao J, Lei Y, Tao S, Lin Q, Chen L, et al. Comprehensive analysis of the cuproptosis-related model to predict prognosis and indicate tumor immune infiltration in lung adenocarcinoma. *Front Oncol* (2022) 12:935672. doi: 10.3389/fonc.2022.935672
- Zhang H, Shi Y, Yi Q, Wang C, Xia Q, Zhang Y, et al. A novel defined cuproptosis-related gene signature for predicting the prognosis of lung adenocarcinoma. *Front Genet* (2022) 13:975185. doi: 10.3389/fgene.2022.975185
- Wang X, Wu S, Liu F, Ke D, Wang X, Pan D, et al. An immunogenic cell death-related classification predicts prognosis and response to immunotherapy in head and neck squamous cell carcinoma. *Front Immunol* (2021) 12:781466. doi: 10.3389/fimmu.2021.781466
- Chen Z, Liu Y, Wu X, Lin W, Liu Z, Huang Y, et al. Spinal CircKcnk9 regulates chronic visceral hypersensitivity of irritable bowel syndrome. *J Pain* (2022). doi: 10.1016/j.jpain.2022.10.007
- Jiang N, Yu Y, Zhang M, Tang Y, Wu D, Wang S, et al. Association between germ-line HLA and immune-related adverse events. *Front Immunol* (2022) 13:952099. doi: 10.3389/fimmu.2022.952099
- Tsvetkov P, Coy S, Petrova B, Dreishpoon M, Verma A, Abdusamad M, et al. Copper induces cell death by targeting lipoylated TCA cycle proteins. *Science* (2022) 375:1254–61. doi: 10.1126/science.abf0529
- Zhan J, Wang P, Li S, Song J, He H, Wang Y, et al. HOXB13 networking with ABCG1/EZH2/Slug mediates metastasis and confers resistance to cisplatin in lung adenocarcinoma patients. *Theranostics* (2019) 9:2084–99. doi: 10.7150/thno.29463
- Liu C, Chikina M, Deshpande R, Menk AV, Wang T, Tabib T, et al. Treg cells promote the SREBP1-dependent metabolic fitness of tumor-promoting macrophages via repression of CD8(+) T cell-derived interferon- γ . *Immunity* (2019) 51:381–397.e386. doi: 10.1016/j.immuni.2019.06.017
- Nechiporuk T, Kurtz SE, Nikolova O, Liu T, Jones CL, D'alessandro A, et al. The TP53 apoptotic network is a primary mediator of resistance to BCL2 inhibition in AML cells. *Cancer Discovery* (2019) 9:910–25. doi: 10.1158/2159-8290.CD-19-0125
- Yu Z, Zhou R, Zhao Y, Pan Y, Liang H, Zhang JS, et al. Blockage of SLC31A1-dependent copper absorption increases pancreatic cancer cell autophagy to resist cell death. *Cell Prolif* (2019) 52:e12568. doi: 10.1111/cpr.12568
- Chen Q, Wang Y, Yang L, Sun L, Wen Y, Huang Y, et al. PM2.5 promotes NSCLC carcinogenesis through translationally and transcriptionally activating DLAT-mediated glycolysis reprogramming. *J Exp Clin Cancer Res* (2022) 41:229. doi: 10.1186/s13046-022-02437-8
- Goh WQ, Ow GS, Kuznetsov VA, Chong S, Lim YP. DLAT subunit of the pyruvate dehydrogenase complex is upregulated in gastric cancer-implications in cancer therapy. *Am J Transl Res* (2015) 7:1140–51. Available at: <https://www.ncbi.nlm.nih.gov/pmc/articles/PMC4532746/>
- Chen S, Cao G, Wu W, Lu Y, He X, Yang L, et al. Mining novel cell glycolysis related gene markers that can predict the survival of colon adenocarcinoma patients. *Biosci Rep* (2020) 40(8):BSR20201427. doi: 10.1042/BSR20201427
- Chen J, Guccini I, Di Mitri D, Brina D, Revandkar A, Sarti M, et al. Compartmentalized activities of the pyruvate dehydrogenase complex sustain lipogenesis in prostate cancer. *Nat Genet* (2018) 50:219–28. doi: 10.1038/s41588-017-0026-3
- Tavera-Montañez C, Hainer SJ, Cangussu D, Gordon SJV, Xiao Y, Reyes-Gutierrez P, et al. The classic metal-sensing transcription factor MTF1 promotes myogenesis in response to copper. *FASEB J* (2019) 33:14556–74. doi: 10.1096/fj.201901606R
- Hao LY, Zhang M, Tao Y, Xu H, Liu Q, Yang K, et al. miRNA-22 upregulates Mtf1 in dorsal horn neurons and is essential for inflammatory pain. *Oxid Med Cell Longev* (2022) 2022:8622388. doi: 10.1155/2022/8622388
- Sabater-Lleal M, Huffman JE, De Vries PS, Marten J, Mastrangelo MA, Song C, et al. Genome-wide association transethnic meta-analysis identifies novel associations regulating coagulation factor VIII and von willebrand factor plasma levels. *Circulation* (2019) 139:620–35. doi: 10.1161/CIRCULATIONAHA.118.034532
- Zhu Y, Wu G, Yan W, Zhan H, Sun P. miR-146b-5p regulates cell growth, invasion, and metabolism by targeting PDHB in colorectal cancer. *Am J Cancer Res* (2017) 7:1136–50. Available at: <https://www.ncbi.nlm.nih.gov/pmc/articles/PMC5446479/>
- Matés JM, Campos-Sandoval JA, Márquez J. Glutaminase isoenzymes in the metabolic therapy of cancer. *Biochim Biophys Acta Rev Cancer* (2018) 1870:158–64. doi: 10.1016/j.bbcan.2018.07.007
- Tong Y, Guo D, Lin SH, Liang J, Yang D, Ma C, et al. SUCLA2-coupled regulation of GLS succinylation and activity counteracts oxidative stress in tumor cells. *Mol Cell* (2021) 81:2303–2316.e2308. doi: 10.1016/j.molcel.2021.04.002
- Riley RS, June CH, Langer R, Mitchell MJ. Delivery technologies for cancer immunotherapy. *Nat Rev Drug Discovery* (2019) 18:175–96. doi: 10.1038/s41573-018-0006-z
- Sun F, Li L, Yan P, Zhou J, Shapiro SD, Xiao G, et al. Causative role of PDLIM2 epigenetic repression in lung cancer and therapeutic resistance. *Nat Commun* (2019) 10:5324. doi: 10.1038/s41467-019-13331-x
- Leone RD, Zhao L, Englert JM, Sun IM, Oh MH, Sun IH, et al. Glutamine blockade induces divergent metabolic programs to overcome tumor immune evasion. *Science* (2019) 366:1013–21. doi: 10.1126/science.aav2588
- Iksen, Pothongsrisit S, Pongrakhananon V. Targeting the PI3K/AKT/mTOR signaling pathway in lung cancer: An update regarding potential drugs and natural products. *Molecules* (2021) 26(13):4100. doi: 10.3390/molecules26134100
- Liu Z, Liu L, Weng S, Guo C, Dang Q, Xu H, et al. Machine learning-based integration develops an immune-derived lncRNA signature for improving outcomes in colorectal cancer. *Nat Commun* (2022) 13:816. doi: 10.1038/s41467-022-28421-6
- Liu D, Schilling B, Liu D, Sucker A, Livingstone E, Jerby-Arnon L, et al. Integrative molecular and clinical modeling of clinical outcomes to PD1 blockade in patients with metastatic melanoma. *Nat Med* (2019) 25:1916–27. doi: 10.1038/s41591-019-0654-5
- Liu Y, Xie P, Jiang D, Liu J, Zhang J, Bian T, et al. Molecular and immune characteristics for lung adenocarcinoma patients with ERLIN2 overexpression. *Front Immunol* (2020) 11:568440. doi: 10.3389/fimmu.2020.568440
- Mcgranahan N, Rosenthal R, Hiley CT, Rowan AJ, Watkins TBK, Wilson GA, et al. Allele-specific HLA loss and immune escape in lung cancer evolution. *Cell* (2017) 171:1259–1271.e1211. doi: 10.1016/j.cell.2017.10.001
- Newman DJ, Cragg GM. Natural products as sources of new drugs over the nearly four decades from 01/1981 to 09/2019. *J Nat Prod* (2020) 83:770–803. doi: 10.1021/acs.jnatprod.9b01285
- Guan Y, Jiang S, Ye W, Ren X, Wang X, Zhang Y, et al. Combined treatment of mitoxantrone sensitizes breast cancer cells to rapalogs through blocking eEF-2K-mediated activation of akt and autophagy. *Cell Death Dis* (2020) 11:948. doi: 10.1038/s41419-020-03153-x

42. Tan BS, Kang O, Mai CW, Tiong KH, Khoo AS, Pichika MR, et al. 6-shogaol inhibits breast and colon cancer cell proliferation through activation of peroxisomal proliferator activated receptor γ (PPAR γ). *Cancer Lett* (2013) 336:127–39. doi: 10.1016/j.canlet.2013.04.014
43. Bala S, Csak T, Saha B, Zatsiorsky J, Kodys K, Catalano D, et al. The pro-inflammatory effects of miR-155 promote liver fibrosis and alcohol-induced steatohepatitis. *J Hepatol* (2016) 64:1378–87. doi: 10.1016/j.jhep.2016.01.035
44. Gao C, Kong N, Zhang F, Zhou L, Xu M, Wu L. Development and validation of the potential biomarkers based on m6A-related lncRNAs for the predictions of overall survival in the lung adenocarcinoma and differential analysis with cuproptosis. *BMC Bioinf* (2022) 23:327. doi: 10.1186/s12859-022-04869-7
45. Ma S, Zhu J, Wang M, Zhu J, Wang W, Xiong Y, et al. A cuproptosis-related long non-coding RNA signature to predict the prognosis and immune microenvironment characterization for lung adenocarcinoma. *Transl Lung Cancer Res* (2022) 11:2079–93. doi: 10.21037/tlcr-22-660
46. Wang F, Lin H, Su Q, Li C. Cuproptosis-related lncRNA predict prognosis and immune response of lung adenocarcinoma. *World J Surg Oncol* (2022) 20:275. doi: 10.1186/s12957-022-02727-7
47. Wang S, Xing N, Meng X, Xiang L, Zhang Y. Comprehensive bioinformatics analysis to identify a novel cuproptosis-related prognostic signature and its ceRNA regulatory axis and candidate traditional Chinese medicine active ingredients in lung adenocarcinoma. *Front Pharmacol* (2022) 13:971867. doi: 10.3389/fphar.2022.971867
48. Chen Y, Tang L, Huang W, Zhang Y, Abisola FH, Li L. Identification and validation of a novel cuproptosis-related signature as a prognostic model for lung adenocarcinoma. *Front Endocrinol (Lausanne)* (2022) 13:963220. doi: 10.3389/fendo.2022.963220